Since January 2020 Elsevier has created a COVID-19 resource centre with free information in English and Mandarin on the novel coronavirus COVID-19. The COVID-19 resource centre is hosted on Elsevier Connect, the company's public news and information website.

Elsevier hereby grants permission to make all its COVID-19-related research that is available on the COVID-19 resource centre - including this research content - immediately available in PubMed Central and other publicly funded repositories, such as the WHO COVID database with rights for unrestricted research re-use and analyses in any form or by any means with acknowledgement of the original source. These permissions are granted for free by Elsevier for as long as the COVID-19 resource centre remains active.

Science of the Total Environment 761 (2021) 143183

Contents lists available at ScienceDirect

Science of the Total Environment

journal homepage: www.elsevier.com/locate/scitotenv

Ozone over Mexico City during the COVID-19 pandemic

Oscar Peralta [a,*], Abraham Ortínez-Alvarez [b,c], Ricardo Torres-Jardón [a], Manuel Suárez-Lastra [d], Telma Castro [a], Luis Gerardo Ruíz-Suárez [a,c]

[a] Centro de Ciencias de la Atmósfera, Universidad Nacional Autónoma de México, Circuito exterior s/n, Ciudad Universitaria, 04510, Coyoacán, Mexico City, Mexico
[b] Posgrado en Ciencias de la Tierra, Universidad Nacional Autónoma de México, Circuito exterior s/n, Ciudad Universitaria, 04510, Coyoacán, Mexico City, Mexico
[c] Instituto Nacional de Ecología y Cambio Climático, Blvd. Adolfo Ruíz Cortines 4209, Jardines en la Montaña, 14210, Coyoacan, Mexico City, Mexico
[d] Instituto de Geografía, Universidad Nacional Autónoma de México, Circuito exterior s/n, Ciudad Universitaria, 04510, Coyoacán, Mexico City, Mexico

HIGHLIGHTS

- Ozone precursor in Mexico City decreased on the lockdown of the COVID-19 pandemic, but its concentration remains the same.
- Satellite data for March – May 2019 and 2020, and surface air quality measurements show similar results.
- Reductions in NOx were so drastic that O_3 formation pass from a VOC sensitive region to a transition-NOx region.

GRAPHICAL ABSTRACT

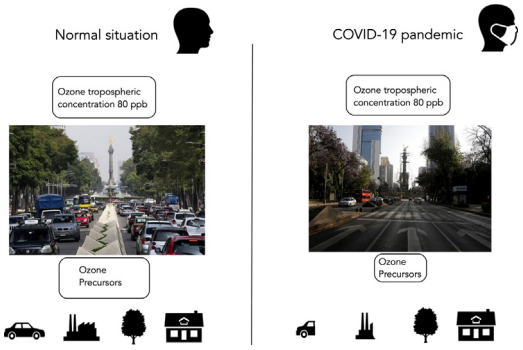

ARTICLE INFO

Article history:
Received 28 May 2020
Received in revised form 6 October 2020
Accepted 12 October 2020
Available online 22 October 2020

Editor: Jianmin Chen

Keywords:
COVID-19
Ozone
Mexico City metropolitan area
Pollutant emissions

ABSTRACT

During the COVID-19 pandemic lockdown, emissions of primary criteria pollutants in the Mexico City Metropolitan Area (MCMA) were substantially reduced, as in many other cities in the world. Unexpectedly, the daily average ozone concentration profile was practically indistinguishable from that of the past two years for the same time span in the calendar. So, we compared surface meteorology data, CO, NOx and O_3 hourly concentrations in the MCMA from the ozone season (from March 1 to May 31) for the years 2018, 2019, and 2020. Also, TROPOMI satellite data on column count of CO, NO_2 and HCHO, above a sparse grid of surface points in the MCMA, were also compared for March, April, and May 2020 with those from 2019. Population density used as a background variable to increase understanding of the observed differences allowed us to propose that reductions in NOx were so drastic that ozone formation moved rapidly from a VOC sensitive region towards a NOx sensitive region. The relevance of that unplanned policy provides impacts of contingent short-term emissions control actions during very high pollution episodes. Further analysis of these and other related data concerning VOC speciation and emissions patterns during the coronavirus lockdown may provide guidelines to enhance emission control policies in the post-COVID-19 times to come.

© 2020 Elsevier B.V. All rights reserved.

1. Introduction

Air pollution makes people more vulnerable to respiratory infections. Around 95% of the planet's population is breathing unhealthy air, according to the annual State of Global Air 2020 (Health Effects Institute, 2020), and Mexico City is not the exception. It has a long history of air quality management challenges. For instance, the Mexican ozone standards were breached in spring 2016 in almost all monitoring stations, both the 1-hour and 8-hour limits (0.095 ppm and 0.070 ppm, respectively) were surpassed. The ozone 1-hour average exceeded the threshold and triggered the local Atmospheric Environmental

* Corresponding author.
E-mail address: oscar@atmosfera.unam.mx (O. Peralta).

https://doi.org/10.1016/j.scitotenv.2020.143183
0048-9697/© 2020 Elsevier B.V. All rights reserved.

Contingency Plan (AECP) on several occasions, leading to the activation of the ACEP which had not been activated in more than a decade (INECC, 2017). The AECP mandates restrictions on mobility and on some business and industrial activities. A year later, in spring 2017, a week of ozone contingencies, from May 15–21, and May 22–24, forced the authorities to reduce mobility in the city. In spring 2018, there were only two contingencies, but the next year we had four more. So, they have been present during the ozone season every year since 2016. In 2020, as observed in other countries, surface air quality data measured by the stations of the MCMA's automatic atmospheric monitoring network (RAMA) from March 1 – May 31 shows a clear decrease in hourly concentrations of NOx and NO_2 as the reduction in urban activities was intensified once the COVID19 lockdown had been officially established (SEDEMA, 2020a, 2020b). However, ozone levels did not show an appreciable decrease. It is not possible to know if VOC levels also decreased, due to the fact that measurements of those ozone precursors are not common, since they are not criteria air pollutants.

Ozone sensitivity in the MCMA region has been recognized as VOC-sensitive, and several authors have explained the lowering in the rate of titration of O_3 by NO and the decrease of NOx in a VOC-limited environment (Dantas et al., 2020; Sicard et al., 2020; Tobías et al., 2020; Gaffney and Marley, 2020). So, a deeper analysis of ozone chemistry sensitivity during the lockdown, based on the principles of the photochemical indicators approach could be used to explain this effect (Sillman and West, 2009; Torres-Jardón and García-Reynoso, 2009; Ying et al., 2009).

The SARS-COV-2 coronavirus appeared in China in December 2019, causing an epidemic in Wuhan. It then spread to all continents and soon after was declared a global pandemic by the World Health Organization (WHO). Mexican authorities suspended school classes in March 23, following the WHO recommendations. Later, on March 30, they declared a health emergency and issued stricter rules aimed at containing the spread of COVID-19 after the number of cases increased. Consequently, vehicular activity decreased, and many people stayed at home. However, people on low incomes and the myriad of informal workers followed those directives with an uneven degree of compliance. As of May 7, the authorities reported 2961 deaths, 29,616 confirmed infections, 7804 confirmed assets, and 18,853 recovered patients.

Vehicle use restrictions, mostly for gasoline cars, and the confinement of people to their homes modified the emissions pattern in the metropolitan area. Those changes in transport activities and oil demand exerted a significant impact on the air quality. Emissions of SO_2, CO, NOx, and volatile organic compounds (VOC) related to gasoline vehicles surely decreased, whereas those related to domestic energy use may have increased. Also, the lockdown happened during the Mexico City's dry season, when forest fires and agricultural burning in the central region of Mexico contributed several ozone precursors.

The use of photochemical models could be of great help in understanding the environmental situation, but one limitation of attempting to explain the ozone formation through modeling is that the exact percentage of potential reductions in both NOx and VOC during the lockdown is unknown. So, satellite-retrieved formaldehyde (HCHO) and nitrogen dioxide (NO_2) column densities have been employed as indicators to investigate spatial and temporal changes in emissions of VOC and NOx around the world as a consequence of the impact of the SARS-CoV-2 pandemic (Muhammad et al., 2020). Besides the typical primary anthropogenic and biogenic HCHO emissions, including those from sporadic biomass burning, the atmospheric oxidation of several volatile organic compounds produces secondary formaldehyde that can be observed spatially and temporally with the Visible Infrared Imaging Radiometer Suite (VIIRS) on board the Sumo-NPP satellite (Wang et al., 2020; Kajino et al., 2019). Thus, the column density of HCHO can be used as a surrogate for the emissions of regional VOC, and the NO_2 column measurements represent both primary NO_2 and oxidation of NO emissions, including NO_2 from the decomposition of PAN transported to the study area. Although natural emissions of NOx may contribute to the burden of these pollutants, anthropogenic emissions surpass those occurring naturally.

If remote sensing of HCHO and NO_2 represent the surrogates for VOC and NOx emissions, then the ratio of HCHO to NO_2 column densities may also indicate the NOx- or VOC-limited ambient ozone formation regime over a long-time horizon in a manner equivalent to their corresponding [HCHO]/[NO_2] determined by using photochemical models (Chang et al., 2016). However, there are limitations for applying the photochemical indicators approach (Kajino et al., 2019). For example, incomplete emissions inventories, local meteorology, and VOC biogenic emissions can alter O_3 production rates.

There were changes on surface and boundary layer emissions during the first three months of the COVID-19 lockdown in MCMA, so we analyzed the available TROPOMI satellite information and surface air quality data during March–May 2018–2020, compared the changes in both the spatial distribution of the column densities of HCHO and NO_2 across the Central Mexico region and the temporal differences in CO, NO_2, NOx, and O_3 concentrations, and we used the results to explain why the ozone in Mexico did not decrease during the COVID-19 lockdown.

2. Methods

The RAMA monitoring network has 22 stations providing hourly information on wind speed and direction, relative humidity, atmospheric pressure, temperature. Eight of these also provide UVA/UVB radiation data. Fig. 1 shows the MCMA grid and the location of RAMA stations.

2.1. Meteorology

Meteorological parameters were compared for 2018, 2019, and 2020 from March 1 (Julian day 60) to May 31 (Julian day 152). We calculate average UV, wind speed and relative humidity data from the 22 air quality stations for every hour each year, in order to know if there were significant changes in wind transport of pollutants from other sites to the MCMA from one year to another.

2.2. Air quality

Hourly average ozone, NOx, NO_2, and CO data were obtained from the RAMA monitoring stations from the period of March 1–May 31, 2018, 2019, and 2020. Information on measurement principles is available from the RAMA website (RAMA, 2020). All monitoring equipment fulfills the requirements of the US EPA related to network monitoring methods. In summary, ozone is measured by the UV photometric method, NOx by the gas phase chemiluminescence method, and CO by non-dispersive infrared photometry (NDIR).

In order to identify whether or not there were changes in emissions of NOx between the two previous years and the year 2020, as well as to observe whether those changes influenced ozone levels, the monitoring data were statistically processed considering five representative monitoring stations located in the northeast (TLA), northwest (SAG), center (MER), southeast (CCA) and southwest (UAX) sectors of the urban area (Fig. 1), as well as a whole considering all the measurement sites. In particular, we focused on both the peaks of CO and NOx during the period 06:00 to 09:00 as indicators of changes in mobile emissions of these precursors group and the afternoon ozone peaks as surrogates for the extent of the photochemical production in MCMA.

On the other hand, in absence of VOC monitoring data during COVID-19, we examined possible differences in the shifts of the cluster-trend for the graph of data points from 06:00 to 09:00 in CO-NOx correlations for the respective medians from all monitoring stations in the MCMA from March to May of the years 2018, 2019 and 2020. The correlation plots may indicate the direction and the magnitude of changes of the VOC/NOx emissions ratio associated with a

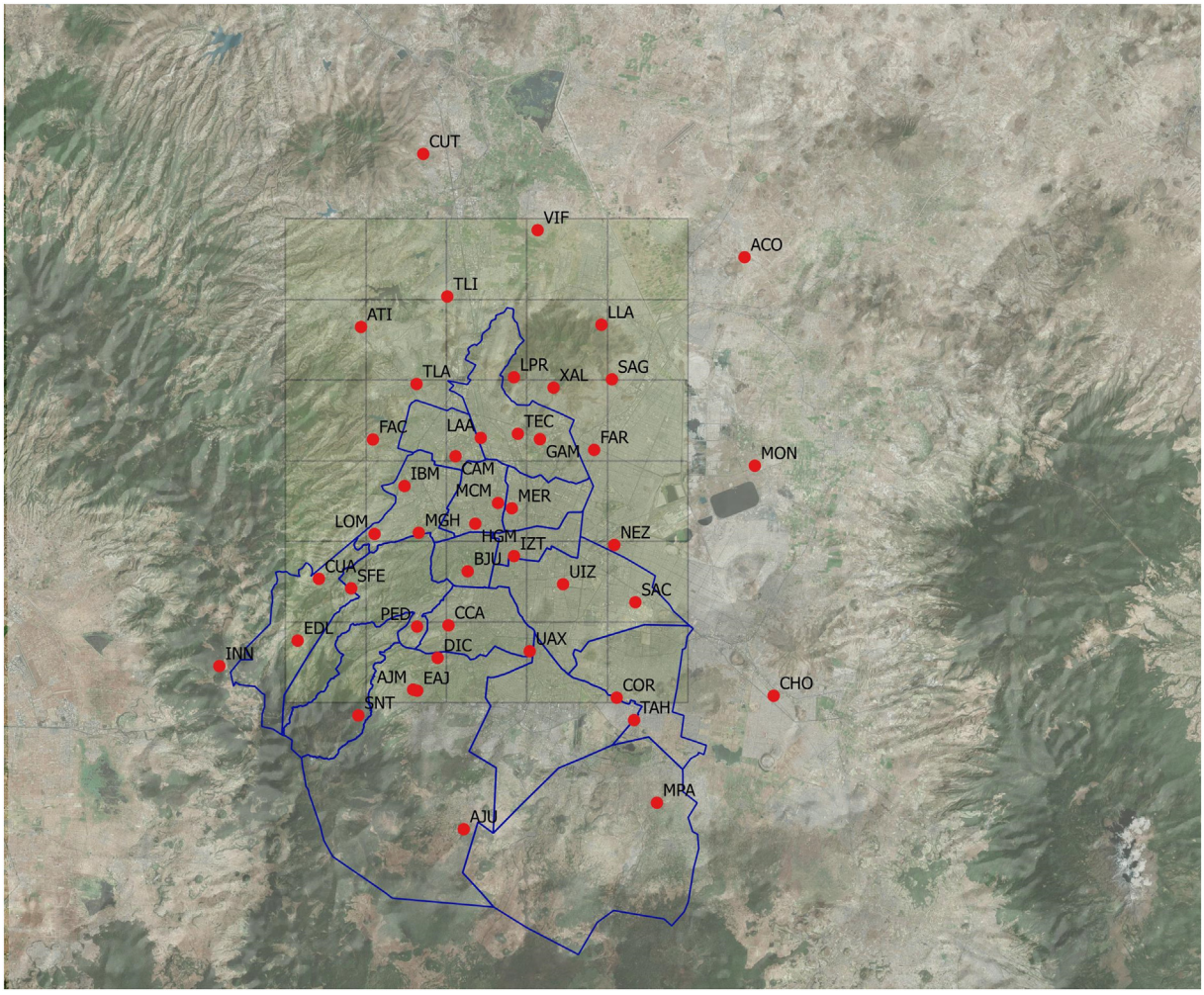

Fig. 1. Cell grid over the Mexico City Metropolitan Area (MCMA). RAMA stations and population were classified based on this grid arrangement.

reduction in transport and other economic activities where combustion is involved. All combustion processes release NOx and a fraction of incomplete burned fuel as CO and VOC. Thus, it could be expected that a change in CO could be related to a proportional change in VOC emissions. The 06:00 to 09:00 monitoring data period corresponds to the peak in urban traffic; besides that, it is the time period when photochemical reactions and the surface mixing layer are still restricted (Fujita et al., 1992). The ambient measurements in the 06:00 to 09:00 period reflect reasonably well on-road vehicular emissions because of the higher contribution of this source category to total emissions. Also, emissions are more uniformly distributed across the urban area.

According to the most recent emissions inventory for MCMA, vehicular emissions contribute around 89% of CO, 82% of NOx, and 18% of VOC to the total burden (SEDEMA, 2018a). However, area sources, mainly evaporative from storage and racking of liquid fuels, leaks of L.P. gas tanks, and use of solvents and other industrial sources, account for nearly 65% of total VOC emissions (SEDEMA, 2017).

We did a *t*-test (two-tail test assuming equal or unequal variances, depending on the F-test of two variances and a *p*-value of 0.05) to test the null hypothesis that the means of the medians of two populations of selected indicators obtained from all the monitoring stations in MCMA for 2020 with respect to the 2018 and 2019 years were not different. The alternative hypothesis was that the means of indicators for the two populations under test were different. The indicators tested were hourly maximum ozone and NOx and the medians of the 06:00 to 09:00. CO and NOx averages, respectively.

2.3. O_3-NOx-VOC sensitivity

Ozone formation is driven by complex nonlinear photochemistry processes and is mainly controlled by VOC and NOx emissions (Sillman and He, 2002; Duncan et al., 2014; Souri et al., 2020). Actions to reduce NOx emission of the main sources will decrease ground-level ozone concentrations in NOx-limited areas but increase ozone concentrations in VOC-limited areas. On the other hand, control strategies to reduce VOC emissions will decrease ozone concentrations in VOC-limited regimens but increase its formation and concentration in NOx-limited areas (Chang et al., 2016).

In order to explain if the processes associated with the maximum average ozone concentrations observed during the three years have changed, an evaluation of the correlation between O_3 and an assumed equivalent NOy was performed based on the concept of photochemical indicators (PI). According to Torres-Jardón and García-Reynoso (2009), the O_3/NOy ratio obtained from air quality models (where NOy includes NOx and the sum of products of its atmospheric oxidation, such as HNO_3, HONO, PAN, and others) has been successfully used as a PI to describe ozone production sensitivity to VOC and NOx in the MCMA when applied to O_3 and NOy measurements. In general, low NOy and high O_3/NOy ratios are associated with ozone production being sensitive to changes in NOx concentrations (NOx-sensitive conditions) and photochemically aged air. High NOy and low O_3/NOy ratios might indicate ozone production being sensitive to changes in VOC concentrations (VOC-sensitive conditions) or relatively fresh emissions of ozone precursors; they are also related to conditions where NOx has been titrated

through reactions of O_3 with directly emitted NO. Because NOy species are not measured by the RAMA in the MCMA, we used surface afternoon NOx measurements as their surrogate (NOy ~ NOx*), based on the fact that NOx concentrations measured by chemiluminescence analyzers usually have a positive bias due to the detection of undefined amounts of HNO_3 and PAN species along with NO_2 (Winer et al., 1974; Dunlea et al., 2007). Therefore, routine NOx measurement may be regarded as a lower boundary of NOy (Blanchard and Fairley, 2001). To define the ozone sensitivity of MCMA during the studied period, the hourly average of ozone and NOx (or NOx*) levels measured between 13:00 and 17:00 at all monitoring sites were plotted on a graph in which the transition value for defining O_3-sensitivity was taken as equivalent to the proposed value of ~8 for the PI: $[O_3]/[NOy]$ by Torres-Jardón and García-Reynoso (2009).

Given that all combustion processes release NOx and a fraction of incomplete burned fuel as CO and VOC, we assumed that in the absence of VOC time series of monitoring data, including during COVID-19, the CO-NOx correlation may indicate the direction change of the VOC/NOx ratio due to a reduction of transport and other economic activities where combustion is involved.

2.4. Satellite images and data

TROPOMI is onboard the Sentinel-5 Precursor (S5P) satellite that orbits along the near-polar sun-synchronous orbit at 824 km above the ground, with a 17 days repeat cycle and equator-crossing time of 13:30 local solar time (LST) on the ascending node. A scanning swath of TROPOMI covers 2600 km wide, providing daily global coverage. It has four two-dimensional spectrometers covering wavelengths from 270 to 2385 nm, which is divided into eight wavelength bands. The third wavelength band, from 320 to 405 nm, is used for HCHO retrieval. The spectral resolution of this wavelength band is about 0.5 nm (FWHM). The spatial resolution of the instrument is 7×7 km^2 at nadir. We also compared data from the Visible Infrared Imaging Radiometer Suite (VIIRS) regarding the impact of forest fires on MCMA air quality. Ultraviolet and visible backscattered solar radiation observations from satellite observations provide relevant information on the lower troposphere of air quality and chemical composition (Apituley et al., 2018; Pedergnana et al., 2018; Henk et al., 2019). The near-surface satellite data, i.e. NO_2 and HCHO, can be used to understand the chemical sensitivity and ozone regimen, i.e. VOC-limited, NOx-limited.

2.5. Geographical data

Data are aggregated in approximately 10 km^2 cells. Population data were obtained by aggregating census tract centroids that fell within each cell. Data correspond to the 2010 census (INEGI, 2010), the most recent population data available at that level. Population data were mapped against CO, NO_2 and HCHO concentrations. Values were obtained by IDW interpolation of the grid centroid values.

3. Results

3.1. Meteorology

The Mexico City Metropolitan Area (MCMA) is among the 10 largest cities in the world with people exposed daily to high pollution outdoor conditions. The city's location in the tropics (19° N) and its altitude (2240 masl) create a high-radiation environment, a condition that drives the chemistry leading to the formation of photochemical ozone. One of the key reactions in ozone formation in the troposphere is the photodissociation of NO_2. The photolysis frequency depends on the solar actinic flux that depends on local optical conditions, including aerosols and gases present in the air above the city (Castro et al., 1997, 2001).

From 20 years of analysis of ozone concentration in the atmosphere, an "ozone season" has been identified in the MCMA, referring to a time of the year in which the concentration of this pollutant reaches the highest levels and also often exceeds the limits of Mexican official standards (SEDEMA, 2018a, 2018b).

High temperatures and intense solar radiation lead to an increase in photochemical activity and favor the formation of ozone. In addition, frequent high-pressure systems and the associated stagnation conditions favor ozone formation (CCA, 2016). This season usually lasts from mid-February to mid-June with its maximums between March and May (SEDEMA, 2018a, 2018b). Table 1 shows the average and standard deviation of most common meteorological parameters involved in ozone formation and pollution transport, and there were no significant changes comparing one year to another.

As usual, during the warm-dry season (March – May) Mexico City experiences high temperatures and low relative humidity, and the meteorological conditions in 2018, 2019, and 2020 were no exception. Wind speed, relative humidity, temperature, UVA, and UVB radiation were not statistically different from one year to another (Carreón-Sierra et al., 2015). A high-pressure system prevents the ventilation of pollutants, favoring the photochemical production of secondary compounds such as ozone, which reach their maximum values after noon (CCA, 2019, 2020). Temperature and UVA radiation data from all stations were used. Both parameters are directly linked to the photolysis of NO_2 and O_3 formation atmosphere. Fig. 2 shows the average of relative humidity, temperatures, UVA and UBV from all stations in the MCMA.

Temperature and UVA radiation data from all stations was used, and both parameters are directly linked to the photolysis of NO_2 and O_3 formation atmosphere.

3.2. Air quality

In the MCMA, ozone concentrations reach risk thresholds very often, between 01:00 and 17:00. Due to the topographical characteristics of the semi-closed basin where the MCMA lies, the morning winds drag most of the pollutants emitted in the north and northeastern areas towards the southwestern-south sector of the basin, where the Sierra de las Cruces and the Sierra Ajusco-Chichinautzin hinder ventilation of the air masses already rich in ozone and other secondary pollutants. The air masses reach the hillsides of the mountains in the afternoon with high levels of O_3. Fig. 3 shows the daily pattern of the medians of hourly averages' NOx and O_3 for the period of March 1 through May 31, 2018, 2019, and 2020 for five representative stations (SAG, MER, TLA, UAX and CCA) and all the monitoring stations in the MCMA.

Fig. 3 shows the medians of hourly averages of NOx and the O_3 for the period of March 15–May 31, 2018, 2019, and 2020 for all the monitoring stations in the MCMA. While there was an average reduction of around 9% at the NOx peak between 2018 and 2019, the peak in 2020 is about 30% lower than the averaged values during two previous years. However, Fig. 3 also shows that the averaged ozone profiles, with a peak at around 80 ppb_v, are indistinguishable during all sunlight

Table 1
Average and standard deviation of relative humidity, temperature, wind speed, UVA, and UVB for ozone seasons (March 1–May 31).

	2018		2019		2020	
	Average	Std. dev.	Average	Std. dev.	Average	Std. dev.
Relative humidity, %	57.22	21.28	53.21	21.10	44.94	19.82
Temperature, °C	16.35	4.87	17.15	4.94	17.44	5.71
Wind speed, m/s	2.00	1.18	2.11	1.23	2.28	1.36
UVA, W/m^2	20.33	16.61	20.10	16.48	22.09	16.58
UVB, W/m^2	0.0898	0.0857	0.1098	0.0957	0.0940	0.0881

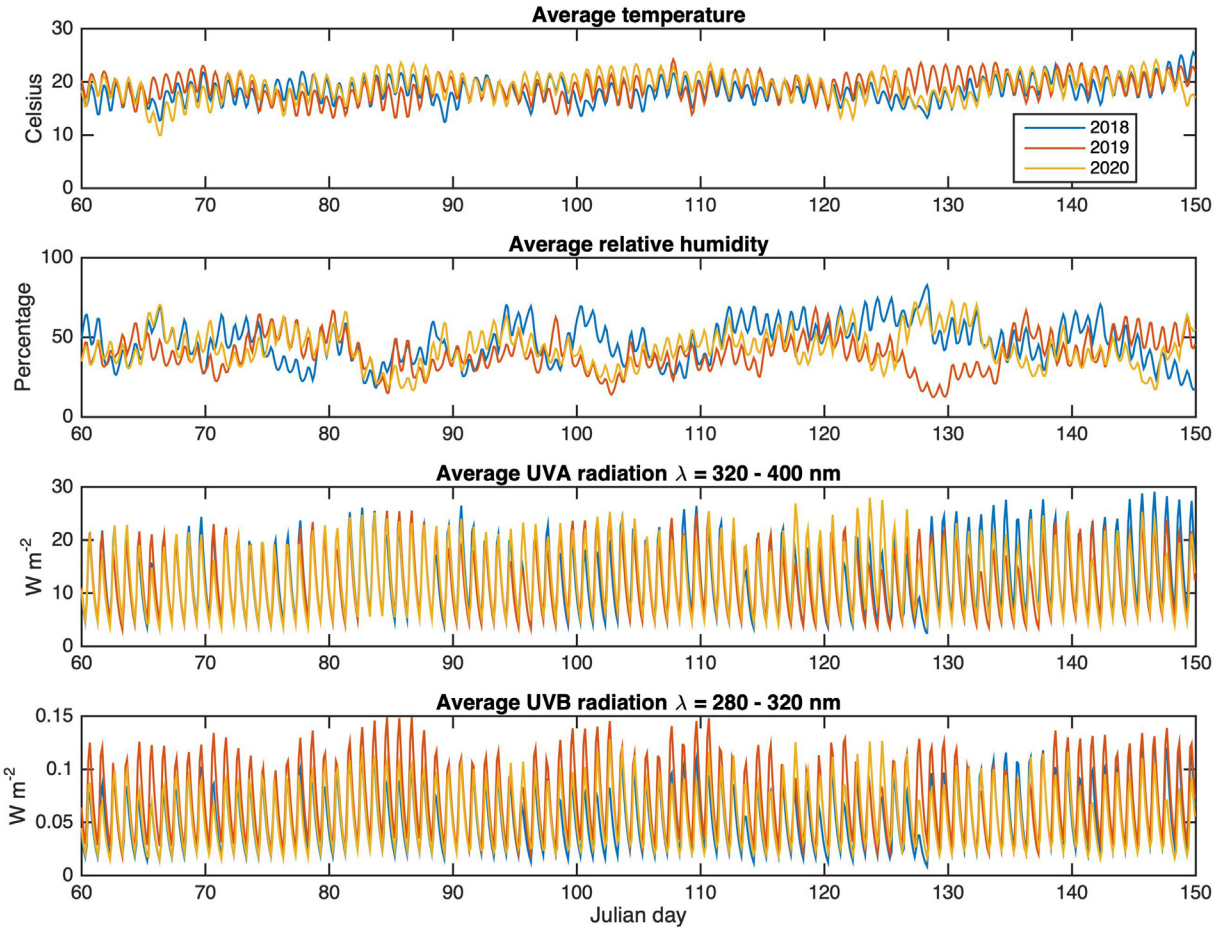

Fig. 2. Average meteorological parameters (temperature, relative humidity, UVA, and UVB) measured by RAMA stations during the ozone seasons of 2018 (blue), 2019 (orange), and 2020 (yellow), from Julian day 60 (March 1) to Julian day 152 (May 31).

hours. The small increases in nocturnal ozone for 2020 are consistent with the lower emissions of NOx during nighttime hours.

The patterns of O_3 and NOx for all sites in Fig. 3 represent reasonably well the hourly variations observed in the representative sites of the MCMA. While there was an average reduction of around 9% at the NOx peak in the medians of all monitoring sites between 2018 and 2019, the peak of the medians in 2020 was 30% lower than peak values during the previous years. The *t*-test showed that there was not a statistically difference between the means of the medians of NOx peaks (at 08:00) for 2018 and 2019 ($p > 0.05$), but there were differences for those years with respect to 2020 ($p \leq 0.05$). Fig. 3 also shows that the O_3 medians profiles for all sites did not change substantially between the three years. The last observation was confirmed with the *t*-test for all the combination of years. The peak for O_3 medians of all stations in the three years was 80 ppb, although the maximum for the 2020 three-month period appeared 1 h earlier than for the peaks for 2018 and 2019. There was also a slight decrease in the 2020 O_3 peaks for TLA and SAG located in the north of the city (representative sites) indicating that upwind regional contributions of ozone were reduced also. The small increases in nocturnal O_3 for 2020 were consistent with the effect of the lower nighttime emissions of NOx during the breakdown, which limited the titration reaction of remaining O_3 by NO.

Fig. 4 shows the 06:00 to 09:00 scatter plots of NOx vs. CO correlations for medians of the hourly averages from all monitoring sites in the MCMA, from March to May for the three years. The hourly ambient CO data available on the SEDEMA database for the MCMA come from instruments whose equivalent EPA method code is less than 500. That implies that they did not have enough resolution to observe changes

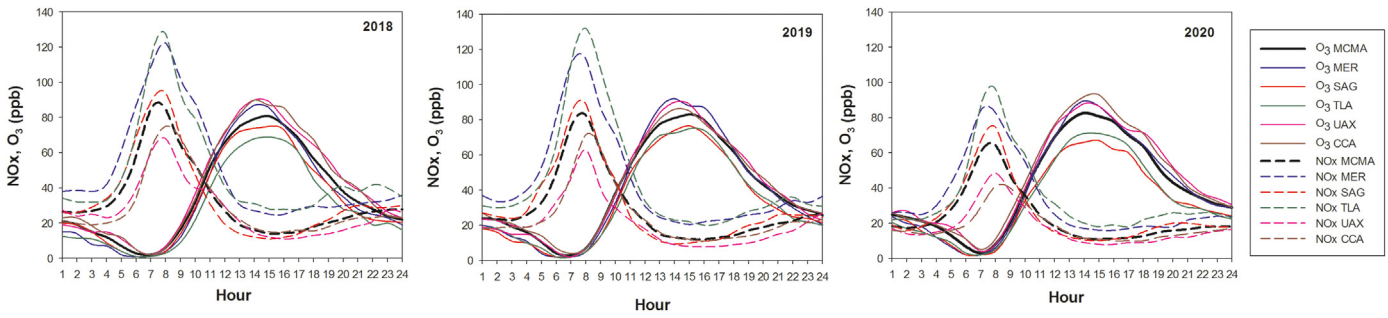

Fig. 3. Daily pattern of the medians for 1-h averages of NOx and O_3 concentrations for all stations (MCMA) and five representative stations in the MCMA for the period of March 1 – May 31 in the years 2018, 2019 and 2020.

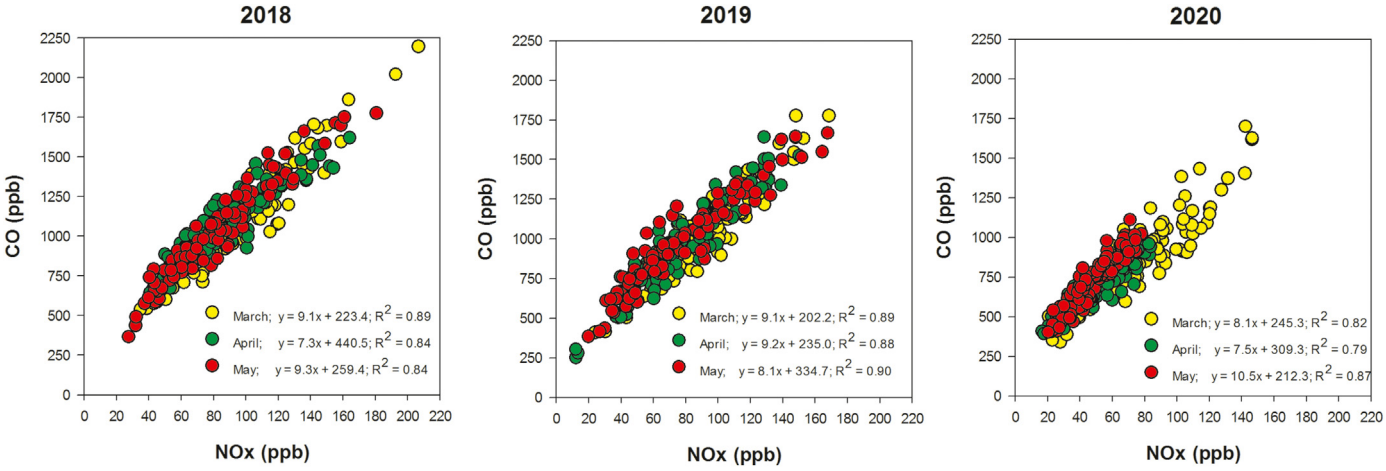

Fig. 4. Correlation scatter plots for 06:00–09:00 a.m. averages of medians for NOx and CO concentrations for all stations in the MCMA during March, April, and May in the years 2018, 2019, and 2020.

below 1 ppm. Those instruments measure CO concentrations at only 0.1 ppm and have in general detection limits of 0.5 ppm which does not represent a problem for evaluating compliance of air quality standards. In fact, data are reported to just one decimal place. In order for the CO data to be useful for our evaluation, we obtained a correction equation from a statistical correlation analysis between hourly data registered with a CO NDIR analyzer typical of the monitoring network and a PICARRO analyzer which measures CO at parts-per-billion (ppb) sensitivity with negligible drift using the Cavity Ring-Down Spectroscopy (CRDS) method, at the same site (CCA station). Hourly data from February to the middle of March 2020 were used for the analysis. CO data from the CRDS analyzer were partitioned into hourly CO intervals of 0.1 ppm according the records from the CO NDIR instrument. The average of each group of CO data for each instrument was calculated resulting seven bins of 0.1 ppm each, plus one additional which included all the CO NDIR concentrations higher than 0.7 ppm. For the correlation analysis, we set a CO dummy value as an equivalent to CO background concentration of 0.1 ppm as the intercept (CO axis) to ensure the background condition. The best coefficient of determination ($R^2 = 0.97$) was obtained with a polynomial regression model ($y = 0.184 + 1.004x - 0.004x$). With this equation, the CO 06:00–09:00 averages of the medians were corrected for all years. We assumed that the correction could represent the CO averages reasonably well.

Fig. 4 shows that the span of data points in 2020 was shorter than previous years, and that trend was stronger from March to May as restrictions on mobility and non-essential activities became stronger while the epidemic progressed. The slopes (ΔCO/ΔNOx) of the correlations for each month in the years 2020 and 2019 were relatively similar between them. Interestingly, the slopes for the months of March and April 2020 were within the range of the slopes for the three months in previous years, but the slope for May 2020 was higher than any of the other months in all years.

The *t*-test performed to identify differences between the 06:00 to 09:00 means of the medians for CO for all data among the three years showed that they were not different to each other, although the difference between 2018 and 2019 was small. However, the *t*-test for the respective 06:00–09:00 means derived from the NOx hourly medians showed strong significant differences between the years 2018–2020 and 2019–2020, while there was no difference in NOx for the 2018–2019 comparison. Table 2 shows the comparison between hourly medians for the three-month period and for each month in the same period for 2018, 2019, 2020, and the associated percent of change for all monitoring stations. From Table 2, it is clear that the percentage of change for the medians of CO and NOx in 2020 was notoriously stronger than that observed in the previous years. NOx differences were even stronger than those for CO. As it was assumed that CO could be a surrogate of VOC emissions, the observed relatively small reduction in ambient CO could indirectly imply that changes in VOC emissions from incomplete combustion in the MCMA were not strong.

Fig. 5 shows the NO_x-O_3-VOC sensitivity indicators analysis for 2018, 2019, and 2020. In 2018, only 6 data pairs of 368 from the afternoon 1-h O_3 and NOx* medians of all MCMA monitoring stations crossed the reference transition line towards the NOx-limited region. In 2019, 24 afternoon data pairs fell in the NOx-limited zone of the graph. However, in 2020, 70 afternoon data pairs crossed the transition line and fell in the NOx limited region.

Apart from NOx and CO, other air pollutants were analyzed. While the average of maximum peak of the hourly medians for $PM_{2.5}$ registered in the MCMA in the years 2018 and 2019 occurred at 10:00 with ~32 μg m^{-3}, the respective average of the hourly peak in the year 2020 was of 25 μg m^{-3} at noon with 28.2 μg m^{-3}. In average, there was a 13% decrease in the hourly averages in 2020 with respect to the years 2018 and 2020 with the occurrence of the higher differences in the averages between the early morning and the noon. Perhaps fewer secondary particles were formed during that period of the day due to the reduction in NOx emissions. For comparison, the WHO guideline 24 h average of 25 μg m-3 for $PM_{2.5}$ was exceeded in 40, 56 and 30 days during the same period for the years 2018, 2019 and 2020, respectively.

Table 2
Analysis of the percentage of changes in 06:00–09:00 a.m. hourly medians of CO and NOx for all monitoring stations in the MCMA for the whole March to May period and for each month in the years 2018, 2019, and 2020.

	Period	CO ppb	NOx ppb	% of change with respect to March of each year	
		Median	Median	CO	NOx
2018	3 months	1044.5	85.3		
	March	1067.5	89.8	0	0
	April	1084.0	86.1	1.54	−4.04
	May	986.3	79.8	−7.61	−11.15
2019	3 months	958.3	76.7		
	March	1012.3	87.6	0	0
	April	927.4	72.7	−8.39	−16.99
	May	938.4	70.0	−7.31	−20.08
2020	3 months	754.8	56.6		
	March	882.0	80.6	0	0
	April	717.5	52.6	−18.65	−34.75
	May	760.6	49.6	−13.76	−38.42

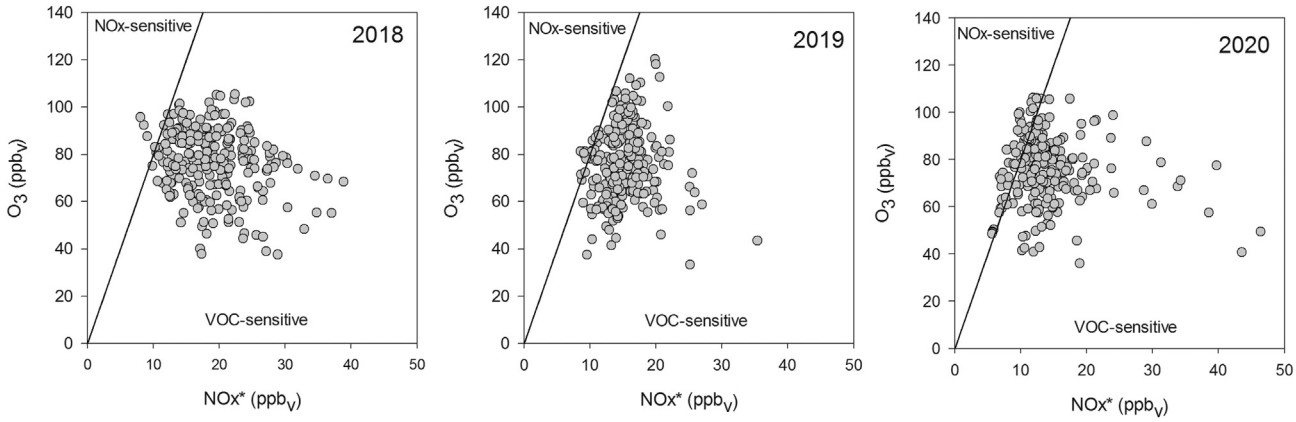

Fig. 5. O_3-NOx-VOC sensitivity indicators analysis for afternoon medians of measured 1-h average O_3 versus NOx* for all MCMA monitoring stations for the period March 1 – May to 31 May in the years 2018, 2019, and 2020. The line represents the transition reference O_3/NOy ratio of 8.0 for the MCMA. The region above the line indicates NOx-limited conditions, while that below represents VOC-limited chemistry.

On the other hand, although the SO_2 levels in MCMA in recent years have been in general low, a slight reduction was observed in 2020 hourly average levels compared with those of 2018 and 2019. The hourly average peak of SO_2 for the years 2019 and 2020 occurred at 10:00 with ~2.9 ppb, while for the year 2018 the peak was 3.7 ppb at the same hour. However, the same reduction observed in the levels of $PM_{2.5}$ in 2020 between the early morning and the time of the peak was also observed for SO_2. It is possible that the number of diesel vehicles in circulation during the breakdown was reduced.

3.3. CO, HCHO, NO_2 column densities

CO, NO_2, and HCHO column data from TROPOMI were collected for a 6×5 grid that covers the MCMA. Data were averaged by cell and month from March – May 2019 and 2020 and analyzed in different ways. Scatter diagrams of NO_2 vs. CO column surface densities for the years 2019 and 2020 are shown in Fig. 6, showing a high data correlation for March 2019 and 2020 ($R^2 \cong 0.80$). However, it decreases strongly in April and May ($0.20 < R^2 < 0.40$). Data span also decreases from March to May in both years, although in a stronger manner in 2020. The slopes also increase each month in 2020 with regard to 2019. Fig. 6 tells a similar story to Fig. 4: emissions are lower in 2020, with stronger reductions in NOx than in CO. However, TROPOMI passes above Mexico City around noon, 2 h later than the nearest hour in Fig. 4. At noon, the surface boundary layer is higher, and turbulence and photochemistry are more active. Also, these effects are stronger as days become sunnier and warmer from March to May. In addition, NOy species start to form scavenging NO_2. All these factors may explain the scatter and poorer correlation in April and May in Fig. 6.

TROPOMI CO column surface density (Fig. 7a) shows a close correlation $R = 0.73$ (2019) and $R = 0.77$ (2020) of population for each grid against the column density of carbon monoxide CO for 2019 and 2020. There are changes in the columns and 2020 is in average 7% lower than the year before. Also, as urban densification increases, CO rises too. Fig. 7b shows that there is a tendency in population growth against the NO_2 column density for both years, but it is not as clear as with CO. However, the 2020 columns are 19% lower on average than 2019. Fig. 7c shows a similar pattern for HCHO, but it is only reduced by 7%. Reducing mobility and economic activities to avoid COVID-19 infections decreased NO_2 emissions, and did affect HCHO (VOC) emissions too, but to a minor degree; therefore, the HCHO/NO_2 ratios for 2020 were larger than those for 2019 as seen in Fig. 5d. If HCHO/NO_2 < 1.5, it is within the VOC limited region, 1.5 < HCHO/NO_2 < 2.3 corresponds to the transition region, and HCHO/NO_2 > 2.3 to the NOx limited region (Chang et al., 2016). On average, the ratio was 1.49 in 2019, whereas it has grown to 1.61 in 2020. This slight change is just enough to displace the system to a transition region.

The MCMA is not uniform in its population density and economic activities, nor in emissions. TROPOMI CO column density data (Figures 8 and 9), representing combustion energy use, showed a larger drop in

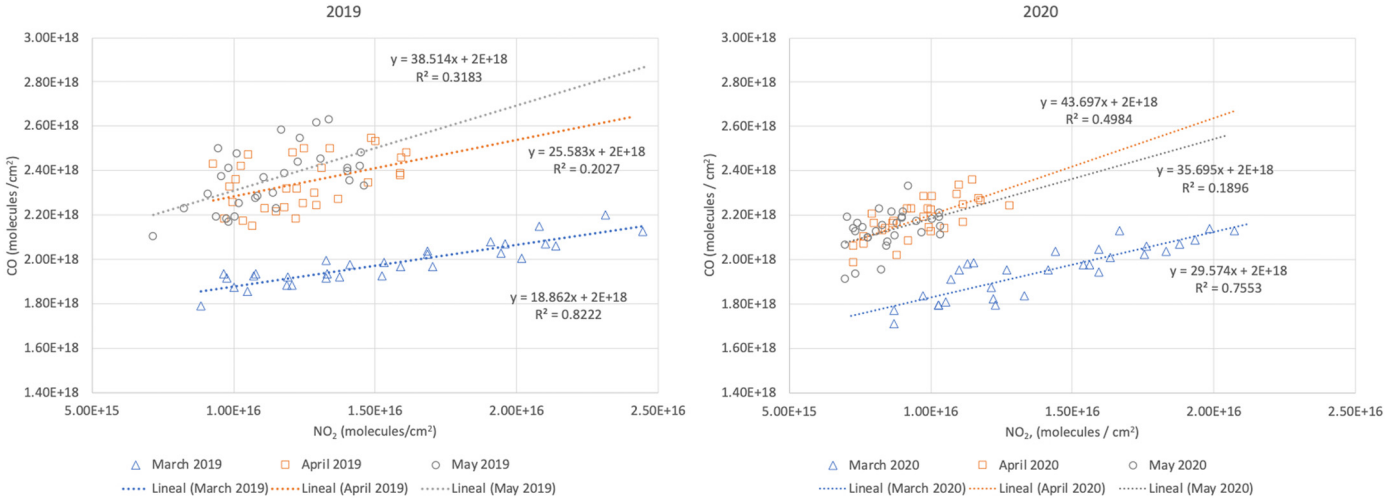

Fig. 6. Scatter plot of NO_2-CO column densities for March–May 2019, and 2020.

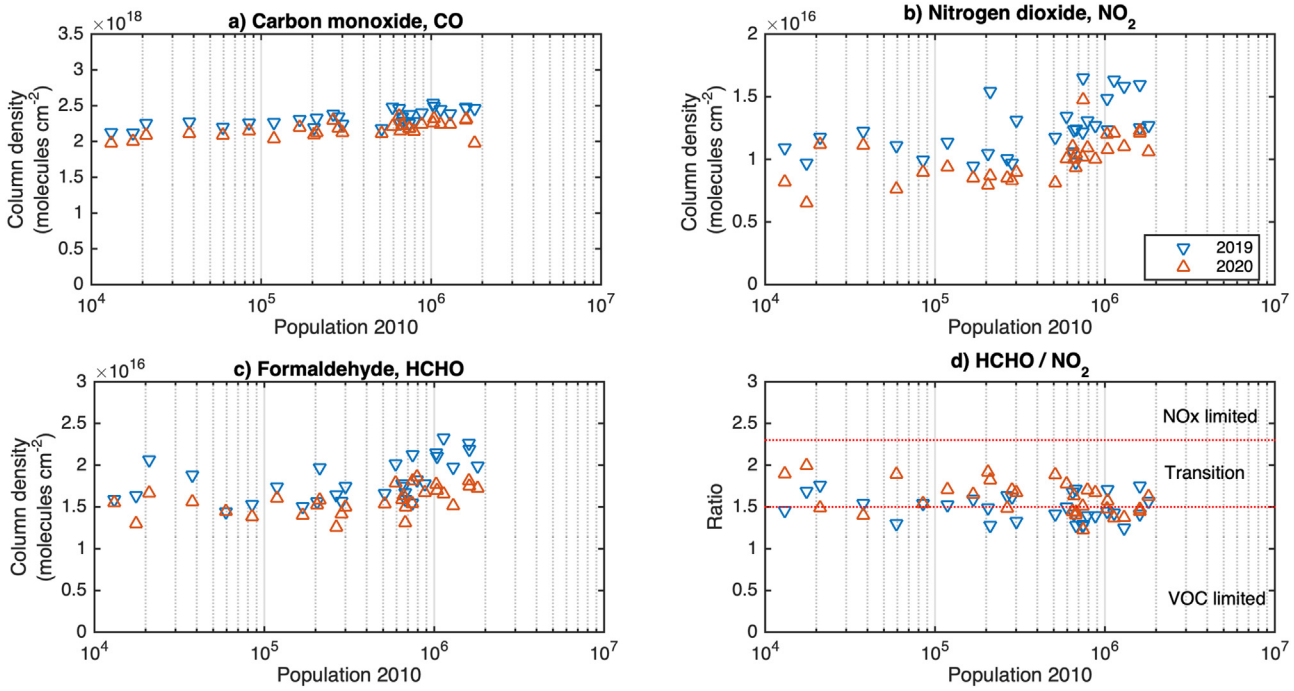

Fig. 7. Column densities of a) CO, b) NO_2, c) CH_2O and d) $HCHO/NO_2$ per population in the grids for 2019 and 2020.

the industrial (northwest) and business (downtown) quarters than in the densely populated residential areas (downtown to east and northeast). A somewhat similar pattern is observed in the NO_2 column map and Table 3. The more affluent parts of the city (downtown to west and southwest) those more able to abide by the stay-at-home directive, show stronger drops in CO and NO_2 column density. In 2019, the HCHO column density map, as a surrogate for VOC, shows higher column densities in the more densely populated areas, in the industrial quarters to the northwest, the financial services quarters from downtown to Santa Fe on the west side and in the forested mountains and the greener and wealthier parts of the city to the west and southwest. The strong reductions in VOC emissions during 2020 show a more uniform distribution but with a stronger color where two or three characteristics of population density, green areas, and wealth tend to coincide. Coarse gradients are products of the sparse cells grid coupled with the interpolation method used.

4. Discussion

It is very likely that the stay-at-home directive, the lockdown of non-essential activities to reduce coronavirus propagation in the MCMA, which included a ban issued on private car use according to the last digit in a car's license plate to further reduce mobility, have displaced the average VOC/NOx ratio to an ozone chemistry region between a transition region or a region sensitive to NOx, as shown in Fig. 5. Also, using CH_2O column density as surrogate for ambient VOC, supports a displacement to a transition to a NOx sensitive regime. Both analyses are consistent in the conclusion that a considerable part of the MCMA is no longer VOC sensitive in this ozone season under lockdown due to the COVID-19 epidemic.

To further understand this unplanned air quality experiment, we assume that the ozone formation chemistry of the MCMA may follow the idealized Empirical Kinetic Modeling Approach isopleths plot as proposed by Sillman and He (2002), which is based on a typical scenario of morning NOx and VOC emissions normalized to the respective extension of the urban area (Fig. 10). Data point A in Fig. 10 represents the assumed average NOx and VOC emissions spatially distributed in the MCMA according to the emissions inventory for the year 2016 (SEDEMA, 2018a, 2018b) and the estimated urban surface area for the same base year. Coincidentally, the data points fall on the 80 ppbv maximum ozone isopleth, about the same as maximum ozone in Fig. 3. To stay in the same ozone isopleth after strong NOx emissions reductions and crossing the transition line to the NOx sensitive region, an increase in VOC may be needed. However, VOC from incomplete combustion should follow the same decrease as that observed for CO. With current data, we cannot distinguish between contributions from domestic, commercial, and mobile sources, but these category sources may not be the origin of the required VOC increase. Indeed, any additional VOC needs first to replace the losses linked to CO reductions and add more to increase the VOC/NOx ratio (Fig. 10).

Where may these necessary VOCs come from? It may be assumed that domestic use of energy for cooking at home did increase, but not enough to compensate for the overall decrease in other sources as observed in the CO map (Fig. 8). VOC from incomplete combustion of GLP in domestic appliances may have increased, whereas those from incomplete combustion of gasoline did decrease. Diesel may have changed less, as in Mexico is mostly used in heavy duty public transport and supplies. However, sanitation guidelines during the lockdown and beyond may have induced an increased use of cleaning products, many of them containing reactive VOC, alcohol, and chloride. Additionally, evaporative VOC emissions need to be taken into account as March and April have been warmer in recent years. The same may be said for biogenic VOC.

Following the approach of the basic graphic tool, we hypothesize that the atmospheric chemistry associated with the unexpected sustainment of a constant maximum ozone average in the MCMA followed the same isopleths observed in previous years.

5. Conclusions

To develop effective strategies for reducing ozone, we need to understand the complex relationship between ozone, VOC and NOx in rural and urban emissions. The persistent lack of data on VOC in ambient air in the MCMA and surrounding areas, together with important

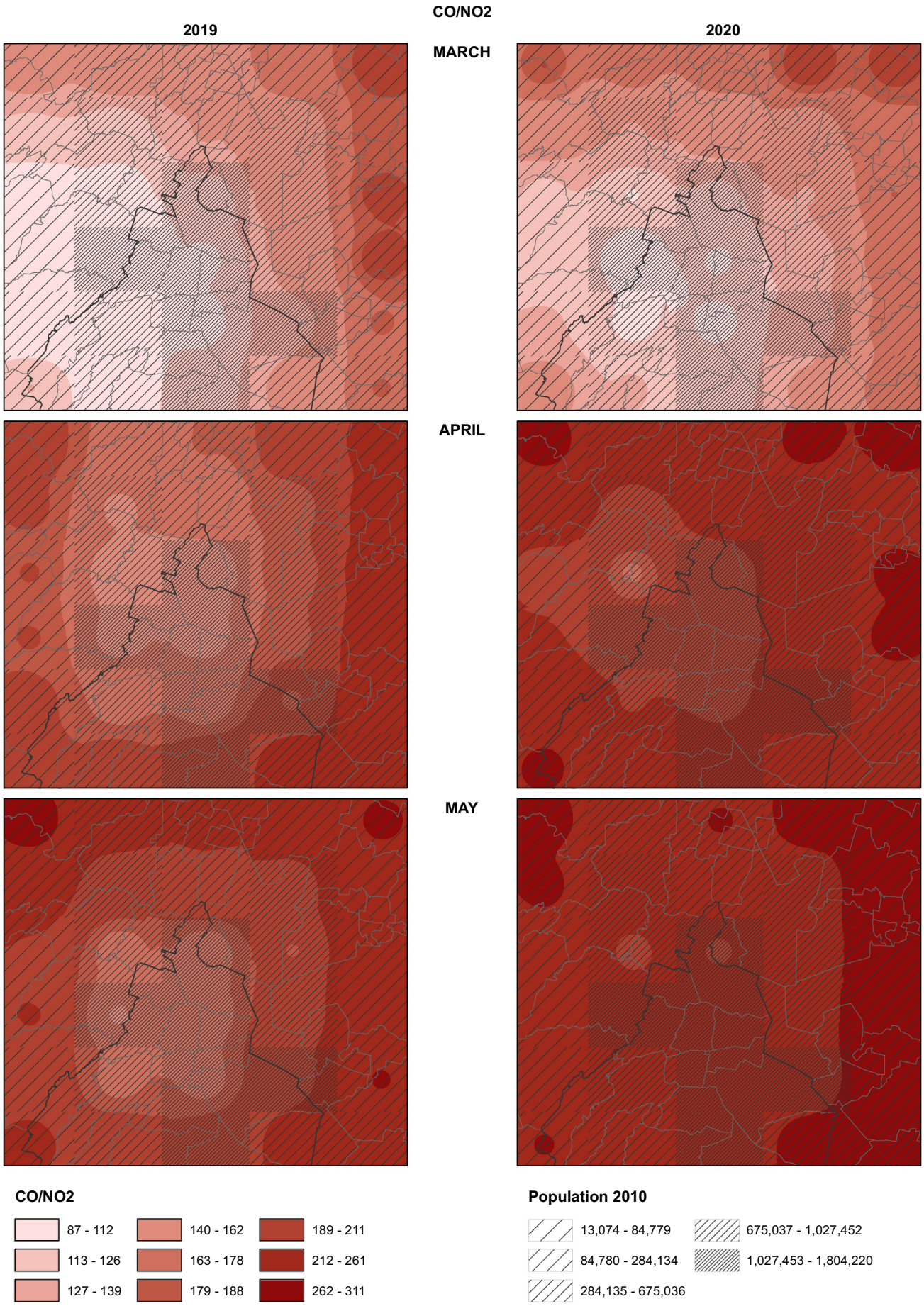

Fig. 8. CO/NO_2 ratio over the population grid in the MCMA.

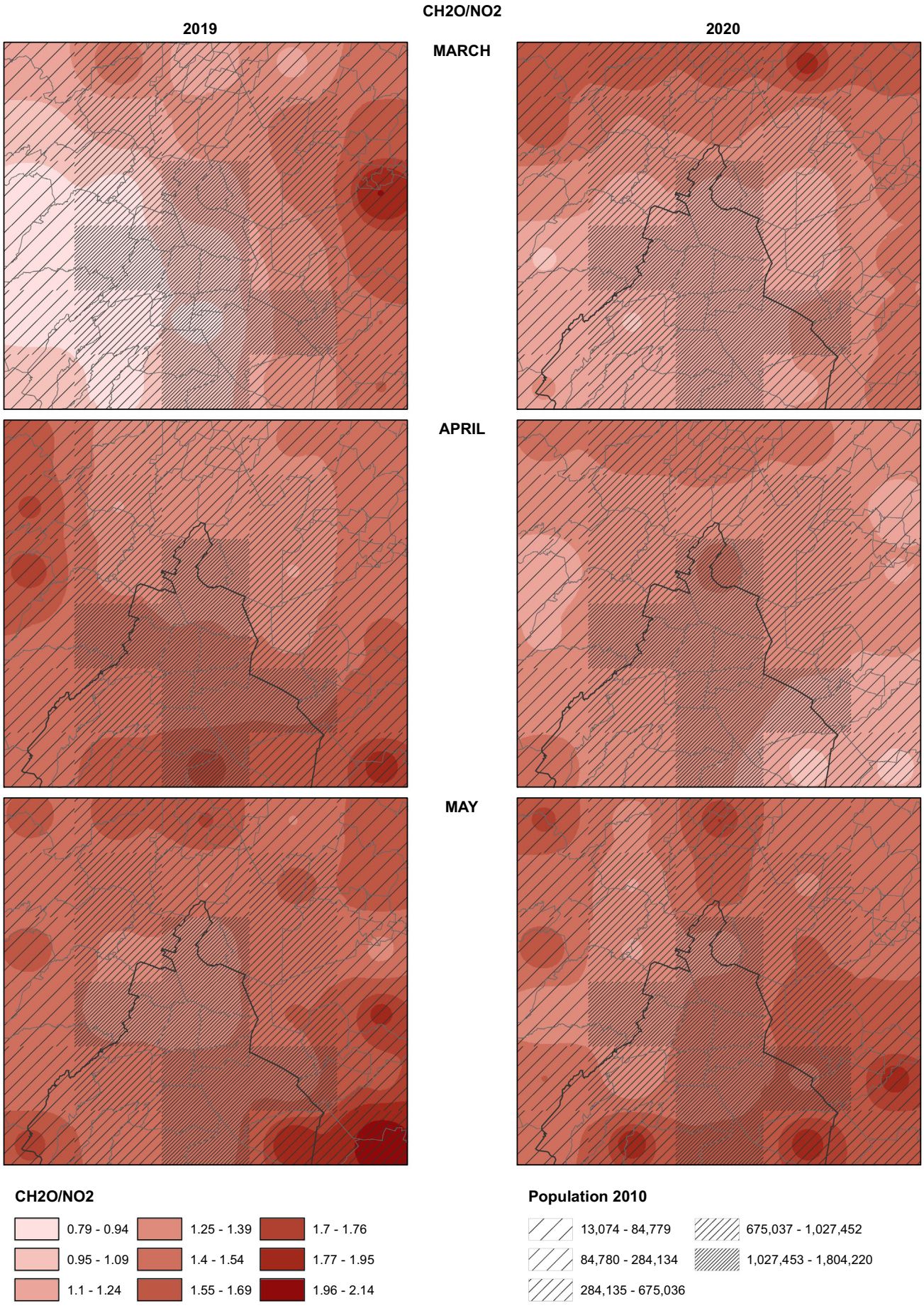

Fig. 9. CH_2O/NO_2 ratio over the population grid in the MCMA.

Table 3
Average ratio for March, April, and May 2019 and 2020, based on TROPOMI satellite information.

	2019			2020		
	March	April	May	March	April	May
CO/NO_2	129	189	209	131	228	251
CH_2O/NO_2	1.14	1.46	1.51	1.29	1.30	1.50
CO/CH_2O	114	129	138	108	176	168

uncertainties in emissions inventories, especially for VOC, are important barriers to defining more focused air quality policy actions. The extension and complexity of the MCMA now require detailed mitigation actions based on scientific evidence.

The analysis we share in this paper falls short of fully explaining this unplanned air quality experiment in MCMA. The analysis needs to be expanded to the complete Megalopolis of Mexico. Available data on mobility from apps or services need to be transferred to modeling-ready emissions inventories to reproduce the observed pollutant concentrations. The same needs to be done for energy consumption and supply, as well as for cleaning and sanitation products. So, lessons need to be learned quickly to contribute to the return to a more sustainable future normality.

Most of Mexico City lives under a volatile organic compound (VOC) limited system; that is, the formation of O_3 has been determined to be in the VOC-sensitive regime, where an increase of VOC leads to a rise in O_3 while an increase in NOx leads to a decrease of O_3. The VOC limited regime frequently occurs in densely populated urban atmospheres. So, the usually high concentration of ambient ozone in Mexico City no longer can be attributed only to vehicles, nor to gasoline composition. A paradigm shift to extend emission control policies to other sources or activities is needed.

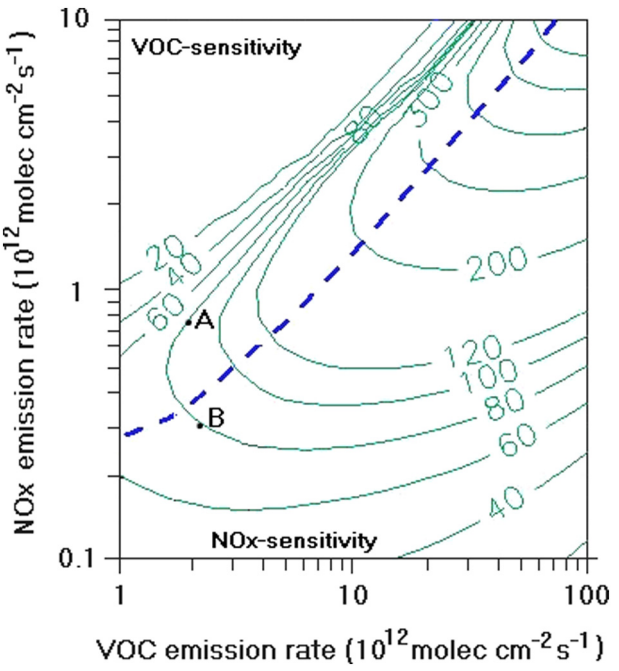

Fig. 10. Schematic representation of the resulting maximum ozone isopleths (ppb) as a function of the initial average emission rate for NOx and VOC. The isopleths (solid green lines) represent conditions during the afternoon. The short blue dashed line represents the transition from VOC-sensitive to NOx-sensitive conditions. Point A represents an idealized scenario for the typical urban environment in the MCMA. Point B may represent the new (VOC, NOx) environmental conditions due to emission reductions as strong as those associated with the COVID-19 lockdown. Isopleths diagram adapted from Sillman and He (2002).

CRediT authorship contribution statement

Oscar Peralta: conceptualization, investigation, and writing; **Abraham Ortínez**: methods, software, formal analysis, investigation; **Ricardo Torres**: writing, methods, formal analysis, investigation; **Manuel Suárez**: methods, formal analysis, visualization; **Telma Castro**: conceptualization, supervision, formal analysis; **Gerardo Ruíz**: conceptualization, supervision, formal analysis.

Declaration of competing interest

The authors declare that they have no known competing financial interests or personal relationships that could have appeared to influence the work reported in this paper.

Acknowledgments

The authors are grateful to Ana Rosa Rosales Tapia, from the Institute of Geography at UNAM, and Miguel Angel Flores Roman, from the National Institute of Ecology and Climate Change, for their help in preparing the maps. Also, to Mexico City's Secretaría de Medio Ambiente for the availability of air quality data.

References

Apituley, A., Pedergnana, M., Sneep, M., Pepijn Veefkind, J., Loyola, D., Landgraf, J., Borsdorff, T., 2018. Sentinel-5 Precursor/TROPOMI Level 2 Product User Manual Carbon Monoxide, SRON-S5P-LEV2-MA-002. Royal Netherlands Meteorological Institute.

Blanchard, C.L., Fairley, D., 2001. Spatial mapping of VOC and NOx-limitation of ozone formation in central California. Atmos. Environ. 35 (22), 3861–3873.

Carreón-Sierra, S., Salcido, A., Castro, T., Celada-Murillo, A.T., 2015. Cluster analysis of the wind events and seasonal wind circulation patterns in the Mexico City region. Atmosphere 6 (8), 1006–1031. https://doi.org/10.3390/atmos6081006.

Castro, T., Ruiz-Suárez, L.G., Molina, J.M., Ruiz Suárez, J.C., Montero, M., 1997. (1997). Sensitivity analysis of UV radiation transfer model and experimental photolysis rates of NO_2 in the atmosphere of Mexico City. Atmos. Environ. 30 (4), 609–620.

Castro, T., Madronich, S., Rivale, S., Muhlia, A., Mar, B., 2001. The influence of aerosols on photochemical smog in Mexico City. Atmospheric Environment. Vol. 35 (1765–1772), 2001.

CCA, 2016. Centro de Ciencias de la Atmósfera. De no Tomarse Medidas Concretas, los Niveles Altos de Ozono se Van a Repetir año Con año: CCA de la UNAM, *Boletín UNAM-DGCS* , p. 305. https://www.dgcs.unam.mx/boletin/bdboletin/2016_305.html.

CCA, 2019. Centro de Ciencias de la Atmósfera. Sobre la Calidad del Aire en la ZMVM. Boletín CCA https://www.atmosfera.unam.mx/sobre-la-calidad-del-aire-en-la-zmvm-14-al-17-de-mayo/.

CCA, 2020. Centro de Ciencias de la Atmósfera. Pronóstico meteorológico http://grupo-ioa.atmosfera.unam.mx/pronosticos/index.php/meteorologia.

Chang, C.Y., Faust, E., Hou, X., Lee, P., Kim, H.C., Hedquist, B.C., Liao, K.J., 2016. Investigating ambient ozone formation regimes in neighboring cities of shale plays in the Northeast United States using photochemical modeling and satellite retrievals. Atmos. Environ. 142, 152–170. https://doi.org/10.1016/j.atmosenv.2016.06.058.

Dantas, G., Siciliano, B., França, B.B., da Silva, C.M., Arbilla, G., 2020. The impact of COVID-19 partial lockdown on the air quality of the city of Rio de Janeiro, Brazil. Sci. Total Environ. 729, 139085.

Duncan, B., Prados, A., Lamsal, L., Liu, Y., Streets, D., Gupta, P., Hilsenrath, E., Kahn, R., Nielsen, J.E., Beyersdorf, A., Burton, S., Fiore, A., Fishman, J., Henze, D., Hostetler, C., Krotkov, N., Lee, P., Lin, M., Pawson, S., Pfister, G., Pickering, K., Pierce, B., R., Yoshida, Y., Ziemba, L, D. (2014). Satellite data of atmospheric pollution for U.S. air quality applications: examples of applications, summary of data end-user resources, answers to FAQs, and common mistakes to avoid, Atmos. Environ., Volume 94, 2014, Pages 647–662, ISSN 1352-2310, doi:https://doi.org/10.1016/j.atmosenv.2014.05.061.

Dunlea, E.J., Herndon, S.C., Nelson, D.D., Volkamer, R.M., San Martini, F., Sheehy, P.M., Zahniser, M.S., M.S., Shorter, J.H., Wormhoudt, J.C., Lamb, B.J., Allwine, J., Gaffney, J.S., Marley, A.N., Grutter, M., Marquez, C., Blanco, S., Cardenas, B., Retama, A., Ramos-Villegas, R.C., Kolb, C.E., C., Molina, L.T., Molina, M.J., 2007. Evaluation of nitrogen dioxide chemiluminescence monitors in a polluted urban environment. Atmos. Chem. Phys. Discuss. 7, 569–604.

Fujita, M.E., Croes, E.B., Charles, L., Bennett, L.Ch., Lawson, R.D., Lurmann, W.F., Main, H.H., 1992. Comparison of emission inventory and ambient concentration ratios of CO, NMOG, and NOx in California's south coast Air Basin. J. Air Waste Manage. Assoc. 42 (3), 264–276.

Gaffney, J.S., Marley, N.A., 2020. Chemistry of Environmental Systems: Fundamental Principles and Analytical Methods. John Wiley and sons, Hoboken, NJ.

Health Effects Institute, 2020. State of Global Air 2020. Special Report. Health Effects Institute, Boston, MA ISSN 2578-6873.

Henk, E., Geffen, Jos van, Boersma, Folkert, Eichmann, Kai-Uwe, Apituley, Arnoud, Pedergnana, Mattia, Sneep, Maarten, Pepijn Veefkind, J., Loyola, Diego, 2019. Sentinel-5 Precursor/TROPOMI Level 2 Product User Manual Nitrogen Dioxide, S5P-KNMI-L2–0021-MA. Royal Netherlands Meteorological Institute INECC, p. 2016. https://www.gob.mx/cms/uploads/attachment/file/112624/Presentacion_Acciones_Adicionales.pdf Last visited site: 08/07/2020.

Instituto Nacional de Ecología y Cambio Climático (INECC), 2017. Informe Nacional de Calidad del Aire 2016, México. Coordinación General de Contaminación y Salud Ambiental, Dirección de Investigación sobre la Calidad del Aire y los Contaminantes Climáticos. Ciudad de México. Diciembre.

INEGI, 2010. Censo de Población Y Vivienda 2010. https://www.inegi.org.mx/programas/ccpv/2010/.

Kajino, M., Hayashida, S., Sekiyama, T.T., Deushi, M., Ito, K., Liu, X., 2019. Detectability assessment of a satellite sensor for lower tropospheric ozone responses to its precursors emission changes in East Asian summer. Sci. Rep. 9 (1), 19629. https://doi.org/10.1038/s41598-019-55759-.

Muhammad, S., Long, X., Salman, M., 2020. COVID-19 pandemic and environmental pollution: a blessing in disguise? Sci. Total Environ. 728, 138820. https://doi.org/10.1016/j.scitotenv.2020.138820.

Pedergnana, M., Loyola, D., Apituley, A., Sneep, M., Veefkind, J.P., 2018. Sentinel-5 Precursor/TROPOMI Level 2 Product User Manual Formaldehyde HCHO, S5P-L2-DLR-PUM-400F, DLR.

RAMA, 2020. Red automática de Monitoreo atmosférico. Secretaría de Medio Ambiente, Gobierno de la Ciudad de México http://www.aire.cdmx.gob.mx/.

SEDEMA, 2018a. Secretaría del Medio Ambiente de la ciudad de México. Inventario de Emisiones de la ciudad de México 2016. Dirección General de Gestión de la Calidad del Aire. Dirección de Programas de Calidad del Aire e Inventario de Emisiones, Mexico City (September).

SEDEMA, 2018b. Calidad del Aire en la cd. de México, Report, 2017.

SEDEMA, 2020a. Secretaría del Medio Ambiente de la ciudad de México. Calidad del Aire. Datos. Dirección de Monitoreo Atmosférico, Ciudad de México Available at. http://www.aire.cdmx.gob.mx/default.php Site last visited: 08/07/2020.

SEDEMA, 2020b. Secretaría de Medio Ambiente de la ciudad de México. Movilidad Durante la Contingencia Por COVID-19 en la ZMVM https://datos.cdmx.gob.mx/pages/mobility-cdmx-covid-dashboard/agregados#sit-cdmx Site last visited: 08/07/2020.

Sicard, P., De Marco, A., Agathokleous, E., Feng, Z., Xu, X., Paoletti, E., Diéguez .J.J., R., Calatayud, V., 2020. Amplified ozone pollution in cities during the COVID-19 lockdown. Sci. Total Environ. 139542.

Sillman, S., He, D., 2002. Some theoretical results concerning O_3-NOx-VOC chemistry and NOx-VOC indicators. Journal of Geophysical Research: Atmospheres (1984–2012) 107 (D22), ACH 26–1-ACH 26-15. https://doi.org/10.1029/2001jd001123.

Sillman, S., West, J., 2009. Reactive nitrogen in Mexico City and its relation to ozone-precursor sensitivity: results from photochemical models. Atmos. Chem. Phys. 9 (11), 3477–3489. https://doi.org/10.5194/acp-9-3477-2009.

Souri, A., Nowlan, C., Wolfe, G., Lamsal, L., Miller, C., González-Abad, G., Janz, S., Fried, A., Blake, D., Weinheimer, J., Diskin, G., Liu, X., Chance, K., 2020. Revisiting the effectiveness of HCHO/NO2 ratios for inferring ozone sensitivity to its precursors using high resolution airborne remote sensing observations in a high ozone episode during the KORUS-AQ campaign, *Atmospheric Environment*. (ISSN: 1352-2310) 224 (2020), 117341. https://doi.org/10.1016/j.atmosenv.2020.117341.

Tobías, A., Carnerero, C., Reche, C., Massagué, J., Via, M., Minguillón, M.C., Andrés Alastuey, A., Querol, X., 2020. Changes in air quality during the lockdown in Barcelona (Spain) one month into the SARS-CoV-2 epidemic. Sci. Total Environ. 138540.

Torres-Jardón, R., García-Reynoso, J., 2009. Assessment of the Ozone-nitrogen Oxide-volatile Organic Compound Sensitivity of Mexico City through an Indicator-based Approach: Measurements and Numerical. https://doi.org/10.3155/1047-3289.59.10.1155.

Wang, J., Zhou, M., Xu, X., Roudini, S., Sander, S., Pongetti, T., Miller, S., Reid, J., Hyer, E., Spurr, R., 2020. Development of a nighttime shortwave radiative transfer model for remote sensing of nocturnal aerosols and fires from VIIRS. Remote Sens. Environ. 241 (2020), 111727 ISSN 0034-4257. https://doi.org/10.1016/j.rse.2020.111727.

Winer, A.M., Peters, J.W., Smith, J.P., James, N., Pitts, J., 1974. Response of commercial chemiluminescence NO-NO_2 analyzers to other nitrogen-containing compounds. Environ. Sci. Technol. 8 (13), 1118–1121 (1974).

Ying, Z., Tie, X., Li, G., 2009. Sensitivity of ozone concentrations to diurnal variations of surface emissions in Mexico City: a WRF/Chem modeling study. Atmos. Environ. 43, 851–885.